Published on 07 January 2015. Downloaded by SEJONG UNIVERSITY on 05/02/2015 08:36:16.

PCCP

PAPER

View Article Online
View Journal | View Issue

Cite this: *Phys. Chem. Chem. Phys.*, 2015, **17**, 5072

Received 25th November 2014, Accepted 7th January 2015

DOI: 10.1039/c4cp05478d

www.rsc.org/pccp

Is hexagonal boron nitride always good as a substrate for carbon nanotube-based devices?†

Seoung-Hun Kang,[a] Gunn Kim*[b] and Young-Kyun Kwon*[a]

Hexagonal boron nitride sheets have been noted especially for their enhanced properties as substrates for sp^2 carbon-based nanodevices. To evaluate whether such enhanced properties would be retained under various realistic conditions, we investigate the structural and electronic properties of semiconducting carbon nanotubes on perfect and defective hexagonal boron nitride sheets under an external electric field as well as with a metal impurity, using density functional theory. We verify that the use of a perfect hexagonal boron nitride sheet as a substrate indeed improves the device performances of carbon nanotubes, compared with the use of conventional substrates such as SiO_2. We further show that even the hexagonal boron nitride with some defects can show better performance as a substrate. Our calculations, on the other hand, also suggest that some defective boron nitride layers with a monovacancy and a nickel impurity could bring about poor device behavior since the imperfections impair electrical conductivity due to residual scattering under an applied electric field.

1 Introduction

The search for substrates to improve the performance of nanoelectronic devices has been an important research topic. Thus far, metals,[1,2] mica,[3] SiC[4,5] or SiO_2[6–10] have been used as substrates. For carbon-based devices, SiO_2 has been most commonly used as a substrate. Although the use of SiO_2 provides many advantages, its primary drawback is to reduce the electronic mobility due to charge density fluctuations induced by the impurities present in the devices.[11,12]

Recently, hexagonal boron nitride (hBN) began to take center stage as a better substrate for graphene-based nanodevices than conventional substrates, such as SiO_2. It has been demonstrated that graphene on the hBN substrate exhibits increased mobility,[13,14] significant improvements in quantum Hall measurements,[14] and enhancement of graphene nanodevice reliability.[15] It has also been shown that carbon nanotube (CNT) based devices on hBN substrates exhibit better device characteristics than on conventional substrates,[16] similarly to graphene-based devices. According to studies based on scanning tunneling microscopy measurements, hBN provides an extremely flat surface with significantly fewer electron–hole puddles than SiO_2.[17,18] In addition to the advantages of providing an atomically smooth surface (relatively free of dangling bonds and charge traps), a large band gap of $\gtrsim 5$ eV,[19] chemical inertness, and a low density of charged impurities, hBN sheets also exhibit an unusual electronic structure that is not observed in most wide band gap materials.

It used to be difficult to fabricate perfect hBN sheets, particularly with a large area, but recently, large-area hBN sheets have been grown by using chemical vapor deposition (CVD).[20–28] A recent intriguing experiment showed that a direct CVD growth of single-layer graphene on a CVD-grown hBN film exhibits better electronic properties than that of graphene transferred onto the hBN film.[29] Thanks to this method, one need not worry about the polymer residues remaining on transferred graphene any longer. However, there still remain two concerns that CVD-grown hBN sheets may possess intrinsic defects, such as vacancies,[30,31] and CNTs may contain metal impurities used as catalysts during their growth,[32–36] which were further explored to confirm the usefulness of hBN substrates.

In this paper, we report a first-principles study of the structural and electronic properties of a semiconducting CNT on defective hBN sheets in the presence of an external electric field (E-field), as well as on a perfect hBN sheet for comparison. For a CNT on a perfect hBN, the E-field shifts the electronic states from the hBN relatively to those from the CNT or to the Fermi level, but the hBN states are still far from E_F, and the CNT states are not altered by the E-field considered. Thereby the perfect hBN may lead to improvement in device performance, compared with conventional substrate materials such as SiO_2, as confirmed by experiments.[13–15,17,18,29] For a CNT on a defective hBN, on the other hand, our study shows that the electronic states originating from the hBN substrate are shifted close to E_F

[a] *Department of Physics and Research Institute for Basic Sciences, Kyung Hee University, Seoul, 130-701, Korea. E-mail: ykkwon@khu.ac.kr*
[b] *Department of Physics, Graphene Research Institute and Institute of Fundamental Physics, Sejong University, Seoul, 143-747, Korea. E-mail: gunnkim@sejong.ac.kr*

† Electronic supplementary information (ESI) available. See DOI: 10.1039/c4cp05478d

This journal is © the Owner Societies 2015

Published on 07 January 2015. Downloaded by SEJONG UNIVERSITY on 05/02/2015 08:36:16.

due to a nickel impurity, which was selected as an exemplary catalyst for CNT growth, and a vacancy in the hBN sheet. Such shifted states and the in-gap states from defects could result in electronic scattering near the Fermi level (E_F) or unwanted electrical conduction (leakage current) through the hBN substrate, causing some critical problems in the CNT based devices.

2 Computational details

We carried out first-principles calculations using the Vienna *ab initio* simulation package (VASP).[37] Projector augmented wave potentials were employed to describe the valence electrons.[38] The exchange–correlation functional was treated within the spin-polarized local density approximation (LDA) in the form of Ceperley–Alder parametrization.[39] The cutoff energy for the plane wave basis was chosen to be 450 eV, and the atomic relaxation was continued until the Hellmann–Feynman force acting on every atom became lower than 0.03 eV Å^{-1}. For more precise calculations, we included the dipole correction.

We first found the equilibrium structure of the hBN sheet with the primitive unit cell, where the B–N bond length d_{BN} was calculated to be 1.44 Å corresponding to the lattice constant of 2.50 Å, which is in excellent agreement with the experimental values of 2.49–2.52 Å.[30,40] To arrange a (10,0) CNT on the pristine hBN sheet, we prepared an orthorhombic supercell with three side lengths of a = 4.32 Å (= $3d_{BN}$), b = 17.5 Å, and c = 25.0 Å, including the rectangular hBN with two sides of a and b and the zigzag CNT placed on the hBN sheet along the a direction. To compensate the discrepancy of their "native" lattice constants along the CNT axial direction, the CNT was elongated by ~5%. The other side lengths, b and c, were selected to be large enough to avoid the intertube interaction from the neighboring cells, and to contain a vacuum region of ~14.4 Å between the top of the CNT and the bottom of the hBN located in the next cell above. For the systems with various vacancies on hBN and/or a Ni impurity, we increased a by a factor of four to be 17.28 Å to ignore the interaction from those defects located in neighboring cells. The Brillouin zone was sampled using a Γ-centered $10 \times 1 \times 1$ ($5 \times 1 \times 1$) k-point mesh for the system with a smaller (larger) a value. The electronic levels were convoluted using Gaussian broadening with a width of 0.05 eV to obtain the DOS.

3 Results and discussion

First, we found the equilibrium stacking configuration of a (10,0) CNT adsorbed onto a perfect hBN substrate. Fig. 1(a)–(c) show three highly-symmetric stacking configurations of the CNT adsorbed onto the hBN sheet similarly in graphite stacking configurations. In AA, some of C_6 hexagonal rings in the CNT are placed to match exactly on the top of B_3N_3 hexagonal rings in hBN. On the other hand, there are two possibilities in AB configuration dissimilar from AB graphite: in AB–B, the hollow sites of the CNT are located at the top of B atoms, while they are at the top of N atoms in AB–N. Our calculations reveal that the most energetically favorable configuration is AB–N stacking, which was also observed as the most stable stacking configuration for graphene on hBN.[41] With respect to the most stable AB–N stacking configuration, AB–B and AA have 61 and 73 meV higher energies, respectively. Therefore, we considered only the AB–N stacking configuration for further investigations. Its projected density of states (PDOS) was calculated to study the effects of an external E-field and a Ni impurity on the electronic structure. The latter was considered since nanoparticulate nickel is often used as a catalyst to synthesize CNTs, and thus the system may contain nickel impurity atoms,[42] unless Ni nanoparticles have been completely removed from the CNT surface or substrate after the growth.

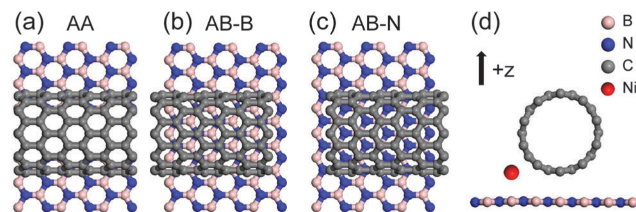

Fig. 1 Three highly-symmetric stacking configurations of a (10,0) CNT adsorbed on an hBN sheet classified similarly in graphite with AA and AB stacking configurations: (a) AA, (b) AB–B (B atoms located at the hollow site of the CNT), (c) AB–N (N atoms at the hollow site) stackings in top view, and (d) in side view. In (d), the arrow indicates the +z direction along which or the opposite of which an external E-field is applied. A Ni impurity atom is also shown in (d). The pink, blue, gray and red spheres represent boron, nitrogen, carbon and nickel atoms, respectively.

Fig. 2(a) shows the PDOS of the pristine AB–N configuration in the absence and the presence of an external E-field. As observed in the middle graph, the conduction band minimum (CBM) and the valence band maximum (VBM) of the hBN, which are respectively located ~2.7 eV above and ~1.5 eV below E_F in the absence of the E-field, are quite far from the CBM and the VBM of the CNT, respectively. As shown in the top (bottom) graph, the external E-field applied along the +z ($-z$) direction shifts the hBN energy bands down (up) noticeably toward the lower (higher) energy relative to those of the CNT due to lower (higher) electrostatic potential on the hBN side. Up to a field strength of 0.2 V Å^{-1}, however, the CBM and VBM of the hBN are located at least 2 eV above and 1 eV below E_F, respectively. Therefore, we conclude that none of the hBN states affect the electronic conduction, regardless of the external E-field, and thus the conduction may occur only through the CNT.

Our results confirm the experimental observations[13,14,17,18] of hBN sheets being much better substrates than conventional ones, such as SiO_2, for CNT or graphene[43] based single-gated field effect transistors (FETs). In a single-gated FET, an applied gate bias generates an E-field between the gate and the channel moving either the VBM or CBM of the hBN close to the counterpart of the CNT, but the energy spacing between them is still kept large, as shown in Fig. 2(a). In a dual-gated FET, however, one gate can be used to control the relative position of the VBM or the CBM of the hBN, while the other to adjust the chemical potential of the CNT channel. This could cause an unexpected output of conduction through not only the CNT channel, but also the hBN substrate.

Published on 07 January 2015. Downloaded by SEJONG UNIVERSITY on 05/02/2015 08:36:16.

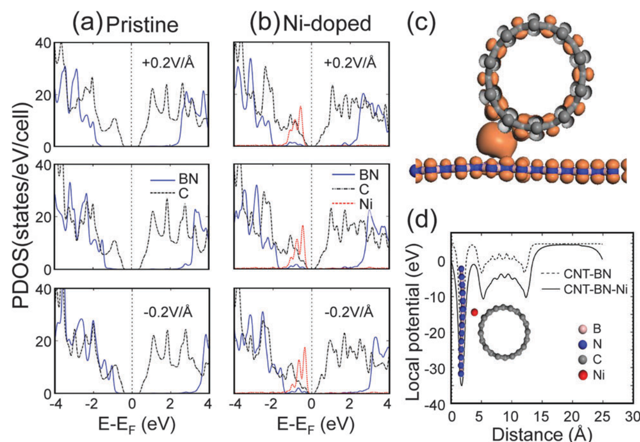

Fig. 2 PDOSs of the (10,0) CNTs deposited on (a) pristine and (b) Ni-doped hBN sheets in the absent (middle) and the presence of an E-field applied with 0.2 V Å^{-1} along the $+z$ (top) and $-z$ (bottom) directions, which are normal to the hBN sheet. In each graph in (a) and (b), a blue solid, a black dash-dotted, and a red dashed lines represent the PDOSs of the hBN, the CNT, and the Ni atom, respectively. The Gaussian broadening of 0.15 eV was used for all PDOSs. There is an arbitrariness to set the Fermi level (E_F) anywhere within the energy gap, we set E_F at the center of the energy gap. (c) Local charge density plotted within the energy window where the strong Ni peaks is observed in the middle graph of (b). (d) Local potential (LP) averaged over a plane parallel to hBN sheet as a function of the distance perpendicular to the sheet. A solid (dashed) line is for the system with (without) the Ni impurity.

Fig. 2(b) shows the PDOS of the Ni-doped AB–N configuration in the absence and the presence of an E-field. Similar to the pristine case, the applied E-field shifts the hBN states up or down by the field directions while keeping them still far from E_F. Just below E_F, however, are there some strongly localized peaks originating from the Ni 3d orbitals, which show no practical change under the applied E-field. In addition, we observed small "satellite" states from the hBN induced by the Ni states and a little modification in the CNT states just below E_F. Our Bader charge analysis showed that 0.26*e* and 0.07*e* have been transferred from the Ni adatom to the CNT and to the hBN, respectively. We also calculated the local charge density corresponding to the localized peaks from the Ni 3d states. As displayed in Fig. 2(c), it exhibits a charge overlapping between the CNT and the hBN through the Ni impurity indicating that the Ni adatom mediates a coupling between the CNT and the hBN sheet. This implies that the nickel atom may play a crucial role as a scattering center when the Fermi level is shifted into this energy window *via* other doping or by applying a gate E-field.

The local potential (LP) was also calculated for the Ni-doped CNT-on-hBN system, as well as the undoped system. Fig. 2(d) shows the calculated LP averaged over a plane parallel to the hBN sheet as a function of the distance normal to the slab. We found that the LP values of the undoped system in the region between the CNT and the hBN appear to be almost the same as those in the vacuum region as represented by a dashed line, indicating that the interaction between the CNT and the hBN sheet may not influence the LP values in between. We can, therefore, conclude that the presence of the hBN sheet does not alter the fundamental response of the CNT when no metal impurity is present. For the Ni-doped system, in contrast, its LP values, plotted with a solid line, appear to be ~5.5 eV lower, compared with those of the Ni-free system with respect to their values in vacuum.

Next, we explored the effects of vacancies existing in the hBN sheet. It was reported that vacancies can be formed during the growth of hBN sheets using the CVD methods.[31] We considered two types of monovacancies: a boron vacancy denoted as V_B and a nitrogen vacancy denoted as V_N; and a kind of multivacancy composed of three boron and one nitrogen empty site (V_{B_3N}), which is one of the two smallest triangular multivacancies.[30] The other triangular multivacancy consisting of one missing B atom and three missing N atoms (V_{BN_3}) was not taken into account because experimental observations showed that more boron atoms are missing than nitrogen atoms and most of the edge-terminating atoms around the vacancies are doubly-coordinated nitrogen atoms.[30] It was found that the CNT prefers to be placed just above V_B and V_N rather than on the perfect hBN region with the energy differences of 0.10 eV and 0.13 eV, respectively. On the other hand, the CNT does not prefer V_{B_3N} to a defect-free hBN region, since the V_{B_3N} defect does not possess broken bonds after the edge reconstruction. To investigate the vacancy effects on the electronic structures, we only considered the configurations in which the CNT is placed on the defect site.

Fig. 3 shows the optimized structures in the top and bottom views of the CNTs on the hBN sheet with V_B, V_N, and V_{B_3N} defects. Their corresponding spin-resolved PDOSs are also shown in the absence and the presence of an applied E-field. Similar to the perfect hBN cases, the applied E-field shifts the hBN states up or down relative to CNT states, depending on the field directions. In Fig. 3(a) for V_B, we found that the Fermi level, E_F, is located just below the VBM of the CNT, which overlaps with that of the hBN. It means that the CNT becomes weakly hole-doped in the presence of V_B. In addition, there exist two localized empty states originating from V_B just above E_F, which exhibit two interesting behaviors. One is that, in response to the E-field, they move in the opposite direction of the other hBN states, *i.e.*, up (down) in energy with the positive (negative) E-field along the z-direction. The other is that these localized states, which are almost completely degenerate at an E-field value of +0.2 V Å^{-1}, become split into two separate states at a value of -0.2 V Å^{-1}. These interesting behaviors are accounted for as follows. Were it not for the CNT, V_B would possess its three-fold symmetry with its three equivalent unsaturated N atoms. In the presence of the CNT, however, the interaction with the CNT, which is very weak, but not negligible, provides a small perturbation breaking its three-fold symmetry lifting its degeneracy. As displayed in PDOSs of Fig. 3(a), such a perturbation becomes weaker and stronger at E-field values of +0.2 V Å^{-1} (top) and -0.2 V Å^{-1} (bottom), respectively, than at no E-field (middle) implying that the positive (negative) E-field tends to weaken (strengthen) the interaction between the hBN and the CNT. Because of the enhanced electronic coupling between the CNT and hBN *via* the boron monovacancy at the negative E-field, unwanted electrical conduction may occur through the hBN sheet.

 This journal is © the Owner Societies 2015

Published on 07 January 2015. Downloaded by SEJONG UNIVERSITY on 05/02/2015 08:36:16.

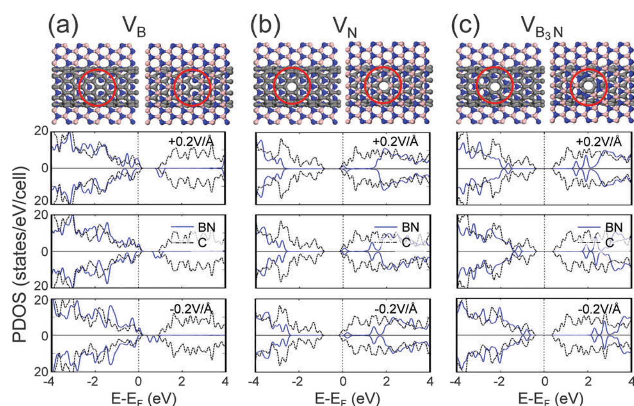

Fig. 3 The optimized structures of (10,0) CNTs placed on top of (a) a boron monovacancy (V_B), (b) a nitrogen monovacancy (V_N), and (c) a triangular multivacancy formed by three missing B and one missing N atoms (V_{B_3N}) created on hBN sheets. For each case, the left (right) configuration is depicted in top (bottom) view. The vacancy in each image is enclosed by the red circle. C, B, and N atoms are denoted by the same color scheme used in Fig. 1. Below these structures are shown their corresponding spin-resolved PDOSs in the absence (middle) and the presence of an E-field applied with 0.2 V Å^{-1} along the $+z$ (top) and $-z$ (bottom) directions. The Gaussian broadening of 0.15 eV was used. While the system with V_B exhibits a magnetic characteristic clearly, those with V_N and V_{B_3N} do not. Note in Fig. 3(b) that an extremely small difference is recognized between majority and minority PDOSs near E_F at $|E|$ = +0.2 V Å^{-1}.

We also observed that the charge distribution near E_F over the hBN is slightly modified and redistributed by the E-field change. The charge redistibution affects the localized states described above, and thus which are shifted up or down by the E-field change.

For the V_N case, in contrast, it was found that the Fermi level is aligned to the CBM of the CNT, which indicates that the CNT becomes weakly electron-doped. Moreover, a very small localized peak from the vacancy appears near E_F as shown in Fig. 3(b). This localized state is much less sensitive to the direction of the applied E-field compared with the case of V_B. In both V_B and V_N cases, those localized states may result in an electronic back-scattering on the CNT surface, since they are located near the VBM or the CBM of the CNT.

For the case of V_{B_3N} in Fig. 3(c), the Fermi level is located in the middle of the gap between the VBM and the CBM of the CNT, and no charge transfer takes place between the CNT and the hBN sheet. As shown in the PDOSs, all of the hBN states including defect states originating from the vacancy are located far from E_F, regardless of the E-field applied. Creating a V_{B_3N} vacancy generates six N atoms surrounding the vacancy, each of which has revealed a dangling bond due to the reduction of its coordination number from 3 to 2. However, these unsaturated bonds get all re-bonded by the edge reconstruction resulting in no dangling bond. This is the reason that no defect state occurs near the E_F of the system with V_{B_3N}. This implies that the presence of such V_{B_3N} vacancies in hBN substrate may not influence the electronic behaviors of CNT based devices. In both V_B and V_N cases, in contrast, there still remain unsaturated dangling bonds at the N and B edge atoms enclosing the respective vacancies corresponding to the defect states near E_F mentioned above.

More interestingly, magnetic properties give rise to the spin magnetic moments calculated to be μ = 1.57 μ_B and μ = 0 for V_B and V_N, respectively. It was found that the magnetic moments have been changed from those of their counterparts without the CNT, which are both μ = 1.00 μ_B[44] meaning that there is apparently one unpaired electron at their respective vacant sites. The results are in agreement with our Bader charge analysis,[45] although it does not give an accurate amount of charge transfer. Δq is defined by the amount of charge transfer to the hBN sheet from the CNT, and is calculated to be 0.49e and $-0.73e$ for V_B and V_N, respectively, where $e = -|e|(<0)$ is an electronic charge. Roughly speaking, the charge of $\sim$0.5e transferred from the CNT increases the spin magnetic moment for V_B, and the electron donation of $\sim$1e to the CNT removes the spin magnetic moment for V_N.

We also explored the dependence of the magnetic moment on the applied E-field. For V_B, the magnetic moment increases (decreases) by 0.18 μ_B (0.31 μ_B) to be μ = 1.75 μ_B (μ = 1.26 μ_B) from μ = 1.57 μ_B at an E-field value of 0.2 V Å^{-1} applied along the $+z$ ($-z$) direction. This E-field dependence is also associated with Δq, which was calculated to be $\sim$0.2e more ($\sim$0.3e less) at an E-field value of +0.2 V Å^{-1} ($-$0.2 V Å^{-1}) with respect to the case with no E-field applied. For V_N, which exhibits zero magnetic moment without the applied E-field, we observed a revival of the magnetic moment, *i.e.*, μ = 0.80 μ_B, at an E-field value of +0.2 V Å^{-1}, implying that 0.8 unpaired electrons have returned to hBN. This is quite consistent with $\Delta q = -0.25e$. At an E-field value of $-$0.2 V Å^{-1}, its magnetic moment is still zero keeping a complete cancellation of one unpaired electron well matching our calculated Δq, which is close to one. All values of the magnetic moments are listed in Table 1. Note that V_{B_3N} retains its nonmagnetic characteristic, regardless of the E-field applied as well as of the presence of the CNT.

Finally, we added a Ni impurity to each of the three systems with respective vacancies V_B, V_N, and V_{B_3N}, described above. Unlike in those systems without a Ni impurity considered above, where the CNT is located directly above each vacant site as shown in Fig. 3, the Ni adatom prefers to sit above the center of each vacant site, and thus prevents the CNT from being placed above the vacant site, The equilibrium configuration of each system is similar to that shown in Fig. 1(d).

Fig. 4 shows the spin-resolved PDOSs of these three systems obtained at three different E-field values, +0.2, 0.0, and $-$0.2 V Å^{-1}. Their hBN states are shifted down (up) in energy under the positive (negative) E-field, which is the same as that seen in Fig. 2 and 3. The VBM and CBM of the hBN are located far from E_F for all the

Table 1 Magnetic moments of undoped or Ni-doped system of a CNT on an hBN sheet with a B or N monovacancy

System	Magnetic moment (μ_B)		
V_B	1.75	1.57	1.26
V_N	0.80	0.00	0.00
Ni + V_B	1.00	1.00	1.00
Ni + V_N	0.54	0.11	0.00
$\lvert E \rvert$ (V Å^{-1})	+0.2	0.0	$-$0.2

Published on 07 January 2015. Downloaded by SEJONG UNIVERSITY on 05/02/2015 08:36:16.

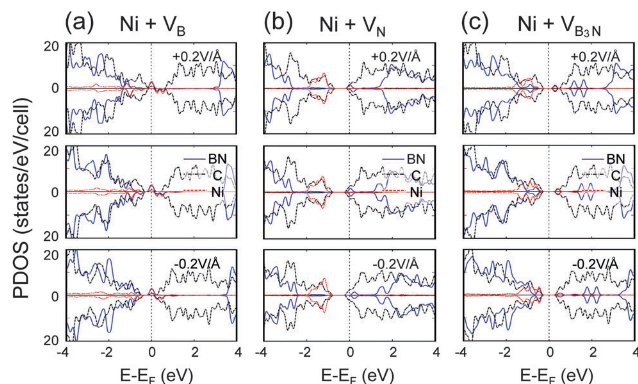

Fig. 4 Spin-resolved PDOSs of the same configurations shown in Fig. 3, but with a Ni impurity placed at (a) V_B, (b) V_N, and (c) V_{B_3N} in the absence (middle) and the presence of an E-field applied with +0.2 V Å^{-1} (top) and −0.2 V Å^{-1} along the *z* direction, normal to the hBN sheet. The Gaussian broadening of 0.15 eV was used for PDOSs.

cases, but defect states are produced by the Ni impurity as well as the vacancy. Especially for the system with the Ni impurity on V_B, it was observed in Fig. 4(a) that some of the defect states are pinned at E_F, and the states from the Ni atom (represented by a red dashed line) are quite strongly hybridized with those from the boron monovacancy (by a blue solid line) in a wide energy range in the valence band. As mentioned earlier, the residual scattering in the CNT-based device may be given rise to by the PDOS peak near E_F formed by strong orbital hybridization between the Ni adatom, the CNT and the hBN sheet. For the one with Ni + V_N or Ni + V_{B_3N}, on the other hand, its electronic structure and its response to the E-field appear to be similar to the counterpart system without a Ni impurity except for the states from the Ni impurity mainly existing relatively deep inside the valence band. It turns out in these two cases that the coupling strength between the Ni impurity and the N or B_3N vacancy is relatively small, compared with that in the Ni + V_B case.

We found that the Ni adatom takes part in determining the magnetic properties of the systems. For V_B, the Ni adatom reduces the magnetic moment exactly to 1 μ_B from 1.57 μ_B. This can be also explained by our Bader charge analysis, which reveals that there is almost no charge transfer to the CNT, but only between the hBN with V_B and the Ni adatom. Those electrons participating in this charge transfer remain as unpaired electrons at the respective parts keeping μ = 1 μ_B. Moreover, its magnetic moment does not respond to the E-field. Such an intriguing magnetic behavior is displayed in the defect states pinned at E_F shown in Fig. 4(a). On the other hand, the Ni adatom converts V_N to be magnetic with the magnetic moment of 0.11 μ_B at zero E-field, while maintaining it nonmagnetic at $|E|$ = −0.2 V Å^{-1}. According to our Bader charge analysis, for Ni + V_N, more electrons are donated to the CNT than for V_N, meaning a complete removal of unpaired electrons from the hBN, but as an exception, at zero E-field, a small amount of electrons is transferred to the hBN from the Ni adatom to make the system weakly magnetic. We also observed that the Ni adatom decreases the magnetic moment to 0.54 μ_B from 0.80 μ_B at an E-field value of +0.2 V Å^{-1}. The charge transfer from the hBN to the CNT is calculated to be 0.49*e*, which is ∼0.24*e* more than that of the system without the Ni adatom. All magnetic moment values are summarized in Table 1. V_{B_3N} remains nonmagnetic, regardless of the existence of the Ni impurity as well as the E-field.

4 Conclusions

In summary, we have studied the effects of an external E-field and a metal impurity on the electronic properties of CNTs on the hBN sheet with and without vacancy defects. For each case, we obtained its electronic structures such as the band structure, projected density of states and local potential. We found that the electronic energy bands of the hBN sheet are shifted in response to the applied E-field, regardless of whether the hBN is perfect or defective with a vacancy, and whether there is a metal impurity or not. However, the shifted electronic states in the valence and conduction bands of the perfect hBN are located still far from E_F under the field strength considered, suggesting that the hBN sheet can be considered as a suitable substrate material for CNT-based single-gate FETs, regardless of the existence of a metal impurity and/or a B_3N vacancy. However, hBN substrates with monovacancies and a metal impurity could exhibit poor performance since the imperfections impair electrical conductivity due to residual scattering when strong top-gate voltage is applied in dual-gate FETs. Our theoretical results are in good agreement with an experimental report that the in-gap states may serve to facilitate residual scattering.[46]

Acknowledgements

We acknowledge financial support from the Korean government through the National Research Foundation (NRF-2011-0016188 and 2013R1A1A2009131). Some portion of our computational work was done using the resources of the KISTI Supercomputing Center (KSC-2013-C1-031).

References

1 S. Marchini, S. Günther and J. Wintterlin, *Phys. Rev. B: Condens. Matter Mater. Phys.*, 2007, **76**, 075429.
2 A. T. N'Diaye, S. Bleikamp, P. J. Feibelman and T. Michely, *Phys. Rev. Lett.*, 2006, **97**, 215501.
3 C. H. Lui, L. Liu, K. F. Mak, G. W. Flynn and T. F. Heinz, *Nature*, 2009, **462**, 339–341.
4 C. Berger, Z. Song, X. Li, X. Wu, N. Brown, C. Naud, D. Mayou, T. Li, J. Hass, A. N. Marchenkov, E. H. Conrad, P. N. First and W. A. de Heer, *Science*, 2006, **312**, 1191–1196.
5 V. W. Brar, Y. Zhang, Y. Yayon, T. Ohta, J. L. McChesney, A. Bostwick, E. Rotenberg, K. Horn and M. F. Crommie, *Appl. Phys. Lett.*, 2007, **91**, 122102.
6 K. Novoselov, A. Geim, S. Morozov, D. Jiang, Y. Zhang, S. Dubonos, I. Grigorieva and A. Firsov, *Science*, 2004, **306**, 666–669.
7 Y. Zhang, Y. Tan, H. Stormer and P. Kim, *Nature*, 2005, **438**, 201–204.

 This journal is © the Owner Societies 2015

Published on 07 January 2015. Downloaded by SEJONG UNIVERSITY on 05/02/2015 08:36:16.

8 Y. Zhang, V. W. Brar, F. Wang, C. Girit, Y. Yayon, M. Panlasigui, A. Zettl and M. F. Crommie, *Nat. Phys.*, 2008, **4**, 627–630.
9 A. Deshpande, W. Bao, F. Miao, C. N. Lau and B. J. LeRoy, *Phys. Rev. B: Condens. Matter Mater. Phys.*, 2009, **79**, 205411.
10 M. Ishigami, J. H. Chen, W. G. Cullen, M. S. Fuhrer and E. D. Williams, *Nano Lett.*, 2007, **7**, 1643–1648.
11 J. Martin, N. Akerman, G. Ulbricht, T. Lohmann, J. H. Smet, K. Von Klitzing and A. Yacoby, *Nat. Phys.*, 2008, **4**, 144–148.
12 Y. Zhang, V. W. Brar, C. Girit, A. Zettl and M. F. Crommie, *Nat. Phys.*, 2009, **5**, 722–726.
13 W. Gannett, W. Regan, K. Watanabe, T. Taniguchi, M. F. Crommie and A. Zettl, *Appl. Phys. Lett.*, 2011, **98**, 242105.
14 C. R. Dean, A. F. Young, I. Meric, C. Lee, L. Wang, S. Sorgenfrei, K. Watanabe, T. Taniguchi, P. Kim, K. L. Shepard and J. Hone, *Nat. Nanotechnol.*, 2010, **5**, 722–726.
15 N. Jain, T. Bansal, C. Durcan and B. Yu, *IEEE Electron Device Lett.*, 2012, **33**, 925–927.
16 A. Baumgartner, G. Abulizi, K. Watanabe, T. Taniguchi, J. Gramich and C. Schnenberger, *Appl. Phys. Lett.*, 2014, **105**, 023111.
17 J. Xue, J. Sanchez-Yamagishi, D. Bulmash, P. Jacquod, A. Deshpande, K. Watanabe, T. Taniguchi, P. Jarillo-Herrero and B. J. Leroy, *Nat. Mater.*, 2011, **10**, 282–285.
18 R. Decker, Y. Wang, V. W. Brar, W. Regan, H.-Z. Tsai, Q. Wu, W. Gannett, A. Zettl and M. F. Crommie, *Nano Lett.*, 2011, **11**, 2291–2295.
19 K. Watanabe, T. Taniguchi and H. Kanda, *Nat. Mater.*, 2004, **3**, 404–409.
20 H. O. Pierson, *J. Compos. Mater.*, 1975, **9**, 228–240.
21 A. S. Rozenberg, Y. A. Sinenko and N. V. Chukanov, *J. Mater. Sci.*, 1993, **28**, 5528–5533.
22 S. Middleman, *Mater. Sci. Eng., A*, 1993, **163**, 135–140.
23 A. C. Adams, *J. Electrochem. Soc.*, 1981, **128**, 1378–1379.
24 W. Auwrter, H. U. Suter, H. Sachdev and T. Greber, *Chem. Mater.*, 2004, **16**, 343–345.
25 F. Mller, K. Stwe and H. Sachdev, *Chem. Mater.*, 2005, **17**, 3464–3467.
26 G. Constant and R. Feurer, *J. Less-Common Met.*, 1981, **82**, 113–118.
27 Y. Shi, C. Hamsen, X. Jia, K. K. Kim, A. Reina, M. Hofmann, A. L. Hsu, K. Zhang, H. Li, Z. Y. Juang, M. S. Dresselhaus, L. J. Li and J. Kong, *Nano Lett.*, 2010, **10**, 4134–4139.
28 K. K. Kim, A. Hsu, X. Jia, S. M. Kim, Y. Shi, M. Hofmann, D. Nezich, J. F. Rodriguez-Nieva, M. Dresselhaus, T. Palacios and J. Kong, *Nano Lett.*, 2012, **12**, 161–166.
29 M. Wang, S. K. Jang, W.-J. Jang, M. Kim, S.-Y. Park, S.-W. Kim, S.-J. Kahng, J.-Y. Choi, R. S. Ruoff, Y. J. Song and S. Lee, *Adv. Mater.*, 2013, **25**, 2746.
30 C. Jin, F. Lin, K. Suenaga and S. Iijima, *Phys. Rev. Lett.*, 2009, **102**, 195505.
31 L. Song, L. Ci, H. Lu, P. B. Sorokin, C. Jin, J. Ni, A. G. Kvashnin, D. G. Kvashnin, J. Lou, B. I. Yakobson and P. M. Ajayan, *Nano Lett.*, 2010, **10**, 3209–3215.
32 M. Pumera, *Langmuir*, 2007, **23**, 6453–6458.
33 P. J. Harris, *Carbon*, 2007, **45**, 229–239.
34 D. Takagi, Y. Homma, H. Hibino, S. Suzuki and Y. Kobayashi, *Nano Lett.*, 2006, **6**, 2642–2645.
35 C. E. Banks, A. Crossley, C. Salter, S. J. Wilkins and R. G. Compton, *Angew. Chem., Int. Ed.*, 2006, **45**, 2533–2537.
36 S. Hofmann, R. Sharma, C. Ducati, G. Du, C. Mattevi, C. Cepek, M. Cantoro, S. Pisana, A. Parvez, F. Cervantes-Sodi, A. C. Ferrari, R. Dunin-Borkowski, S. Lizzit, L. Petaccia, A. Goldoni and J. Robertson, *Nano Lett.*, 2007, **7**, 602–608.
37 G. Kresse and J. Furthmüller, *Phys. Rev. B: Condens. Matter Mater. Phys.*, 1996, **54**, 11169–11186.
38 G. Kresse and D. Joubert, *Phys. Rev. B: Condens. Matter Mater. Phys.*, 1999, **59**, 1758–1775.
39 D. M. Ceperley and B. J. Alder, *Phys. Rev. Lett.*, 1980, **45**, 566–569.
40 W. Paszkowicz, J. Pelka, M. Knapp, T. Szyszko and S. Podsiadlo, *Appl. Phys. A: Mater. Sci. Process.*, 2002, **75**, 431–435.
41 G. Giovannetti, P. Khomyakov, G. Brocks, P. Kelly and J. van den Brink, *Phys. Rev. B: Condens. Matter Mater. Phys.*, 2007, **76**, 073103.
42 X. Liu, V. Gurel, D. Morris, D. Murray, A. Zhitkovich, A. Kane and R. Hurt, *Adv. Mater.*, 2007, **19**, 2790–2796.
43 S. Park, C. Park and G. Kim, *J. Chem. Phys.*, 2014, **140**, 134706.
44 B. Huang and H. Lee, *Phys. Rev. B: Condens. Matter Mater. Phys.*, 2012, **86**, 245406.
45 W. Tang, E. Sanville and G. Henkelman, *J. Phys.: Condens. Matter*, 2009, **21**, 084204.
46 S. Droescher, C. Barraud, K. Watanabe, T. Taniguchi, T. Ihn and K. Ensslin, *New J. Phys.*, 2012, **14**, 103007.